Registration of the transition radiation with GaAs detector: Data/MC comparison

Registration of the transition radiation with GaAs detector: Data/MC comparison

J Alozy[1], N Belyaev[2], B L Bergmann[3], T R V Billoud[3], P Broulim[4], P Burian[3,4], M Campbell[1], G Chelkov[5], M Cherry[6], F Dachs[1,7], S Doronin[2], K Filippov[2], P Fusco[8,9], F Gargano[9], E H M Heijne[1,3], S Konovalov[10], X Llopart Cudie[1], F Loparco[8,9], M N Mazziotta[9], L Meduna[3], H Pernegger[1], D Ponomarenko[2], S Pospisil[3], D Rastorguev[5], C Rembser[1], A Romaniouk[2], A A Savchenko[2,11,12], E J Schioppa[13], S Smirnov[2], Y Smirnov[2], P Smolyanskiy[3], P Spinelli[8,9], M Strikhanov[2], P Teterin[2], V Tikhomirov[10], K Vorobev[2] and K Zhukov[10]

[1] CERN
[2] National Research Nuclear University MEPhI
[3] Institute of Experimental and Applied Physics, Czech Technical University in Prague
[4] Faculty of Electrical Engineering, University of West Bohemia in Pilsen
[5] Joint Institute for Nuclear Research
[6] Louisiana State University
[7] Technical University of Vienna
[8] INFN Bari
[9] Dipartimento di Fisica "M. Merlin" dell'Università e del Politecnico di Bari
[10] P. N. Lebedev Physical Institute of the Russian Academy of Sciences
[11] Belgorod National Research University, 85, Pobedy St., Belgorod, 308015, Russia
[12] National Research Center Kurchatov Institute
[13] Università del Salento, Dipartimento di matematica e fisica "E. De Giorgi" and INFN Lecce

E-mail: Anatoli.Romaniouk@cern.ch, NLBelyayev@mephi.ru

Abstract. New developments of pixel detectors based on GaAs sensors offer effective registration of the transition radiation (TR) X-rays and perform simultaneous measurements of their energies and emission angles. This unique feature opens new possibilities for particle identification on the basis of maximum available information about generated TR photons. Results of studies of TR energy-angular distributions using a 500 μm thick GaAs sensor attached to a Timepix3 chip are presented. Measurements, analysis techniques and a comparison with Monte Carlo (MC) simulations are described and discussed.

1. Introduction

Transition Radiation Detectors (TRDs) are widely used for electron-hadron separation in both accelerator and cosmic-ray experiments (see reviews [1–3]). With growing energies of modern and planned accelerators there is also a need to separate hadrons in the TeV energy range [4]. Transition radiation is produced when a highly relativistic particle crosses the interface between materials of different refractive index. In the X-ray range, the TR yield strongly depends on the particle gamma factor and manifests a sort of threshold effect, i.e. it becomes significant at

gamma factors above a threshold γ_{thr}. For multiple interfaces, it saturates and reaches almost a plateau at γ_{sat}. The TR X-rays, ranging from a few keV to a few tens keV, are emitted in a forward direction at small angles (within a few mrad) with respect to the particle trajectory. There are a few important properties of TR which should be taken into account when designing a TRD for particle identification. One of them is the fact that the energy spectrum of TR produced in radiators with foils thicker than 40 μm exhibits a few peaks, which have different gamma dependencies [5, 6]. Another one is the actual angular distribution of TR photons. The most probable production angle of the TR photons belonging to the most energetic peak of the energy spectrum has a specific dependence on the gamma factor [7]:

$$\theta \approx \sqrt{1.4\pi^2/\gamma_{sat}^2 - 1/\gamma^2}. \quad (1)$$

Equation (1) shows that the larger gamma factor is, the larger the TR emission angle is. Usually only the energy information about TR photons is used in TRDs; however, a simultaneous measurement of the number of X rays, their energies and the angles at which they are produced can enhance the particle identification (PID) efficiency of a TRD. The major drawback for using the angular information is the separation of the absorbed photons from the particle track, which requires high-granularity detectors. An increase of the TR saturation point (or the extension of the gamma factor range) requires the increase of the foil thickness and this unavoidably leads to the increase of TR photon energies up to a few tens of keV. In that case photon detectors with a high absorption efficiency must be used. The development of high granularity pixellated ASICs [8] connected to thick and/or high Z semiconductor sensors opens new possibilities to create efficient TR detectors with a good separation of the charged particle and TR photons.

Some results of TR measurements and detailed comparison with MC simulations using a 480 μm thick Si-sensor attached to a Timepix3 chip were presented in [7]. Si-sensor can be effectively used only for registration of TR photons with energies up to about 15 keV. For larger energies, materials such as GaAs or CdTe should be used. CdTe detectors exhibit the largest efficiency of photon absorption, but also a very large probability (close to 85%) of fluorescent photon production with energies of about 23 keV (Cd) and 27.2 keV (Te). Such photons have relatively large absorption length (about 110 μm for Cd and 59 μm for Te) and might be absorbed far from a TR interaction point, or even escape from the detector volume. This will lead to a deterioration of the information about the TR photon energy and production angle. From that point of view the most promising material to be used in the TRD is GaAs. Preliminary results of a comparison of the TR measurements made with Si and GaAs pixel sensors attached to the Timepix3 chip were published in [9].

A dedicated model of the detector operation is a very important component of the detector development. In this paper, the measurements and the detector MC model are described. The results are compared for radiators made from 30 or 90 Mylar foils of 50 μm thickness, spaced by 2.97 mm for 20 GeV/c electron beam.

2. Experimental setup

Studies were carried out at the CERN SPS facility with 20 GeV/c electrons and muons from 120 to 290 GeV/c using different types of radiators. The test beam set-up is shown schematically in figure 1.

It consists of multi-foil radiators positioned at about 2 m distance from the detector. A helium filled pipe was placed in-between to prevent the absorption of emitted TR photons in air. A chromium-compensated GaAs (GaAs:Cr [10]) 500 μm thick sensor bonded to the Timepix3 chip [11] was used as a detector. The chip is a square matrix of 256×256 pixels with a pixel pitch of 55 μm. The bias voltage applied to the sensor was −450 V. The Katherine interface was used to read information from the Timepix3 chip [12]. The Timepix3 chip was operated

in a data driven mode. Test beam setup was instrumented with a set of ancillary detectors for PID consisting of upstream Cherenkov counter, preshower detector and lead glass calorimeter. Hardware triggers were implemented to select the various types of beam particles, and a flag corresponding to each trigger was added in the data stream. This allows to make offline selection of data corresponding to different sorts of particles.

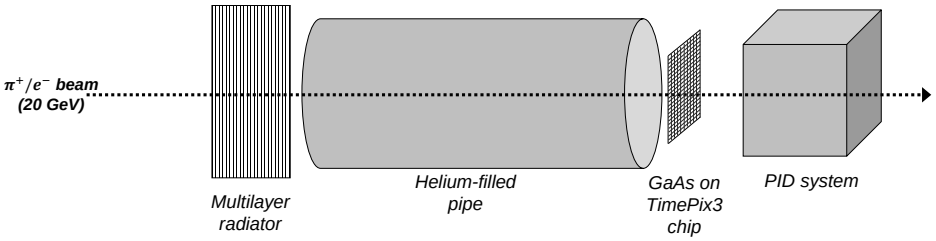

Figure 1. A sketch of the test beam setup at the CERN SPS.

The GaAs detector was calibrated pixel-by-pixel using fluorescence lines of different elements. The photon calibration is limited to energy of 5.95 keV (Fe^{55}). The data point were fitted by the function $ToT(E) = a\,E + b - \frac{c}{E-t}$, where a, b and c are fit parameters while t is the minimum threshold energy which can be detected [13]. The threshold for each pixel during the calibration and the test beam measurements was set to 4.2 keV.

An essential property of the Timepix3 ASIC is the recording of the time of incidence with 1.6 ns precision in each pixel. Using these time stamps for the clusters and trigger, it is easy to correlate the relevant TR photon conversions with the parent particle, by looking within a time window of a few hundreds of ns. This time window was used to combine all fired pixels into an event.

3. Data analysis

Within the event, pixels are clustered with an algorithm based on the telescope reconstruction software "Proteus" [14]. A cluster is defined as a group of adjacent pixels with a signal above the threshold which have a common side or connected in corners. Clusters are separated by empty pixels. Once all pixels have been grouped into clusters, cluster energies are calculated by summing up the energies of all pixels. The position of a cluster in local plane coordinates is assigned by calculating the energy-weighted average of the individual pixel positions, i.e.:

$$x_{COG} = \frac{\sum_{j=1}^{n} \omega_j x_j}{\sum_{j=1}^{n} \omega_j},\ y_{COG} = \frac{\sum_{j=1}^{n} \omega_j y_j}{\sum_{j=1}^{n} \omega_j}, \tag{2}$$

where n is the number of pixels in the cluster, ω_j is the energy of the j-th pixel in the cluster and (x_j, y_j) are its coordinates. The suffix "COG" stands for "center of gravity".

In figure 2 (a) a scatter plot of cluster energy against the number of pixels in the cluster is shown. Clusters with energies exceeding 180 keV correspond to beam particles. TR clusters are grouped at lower energies and smaller cluster sizes. Only events in which one cluster above 180 keV is present were considered valid for analysis. In figure 2 (b) the distribution of the number of reconstructed TR clusters in a single event is shown. The average number of reconstructed clusters for the 90 Mylar foil radiator is 2.8. When all clusters are reconstructed, their distances to the beam particle cluster are calculated and the emission angles are obtained using the distance between the detector plane and the radiator center.

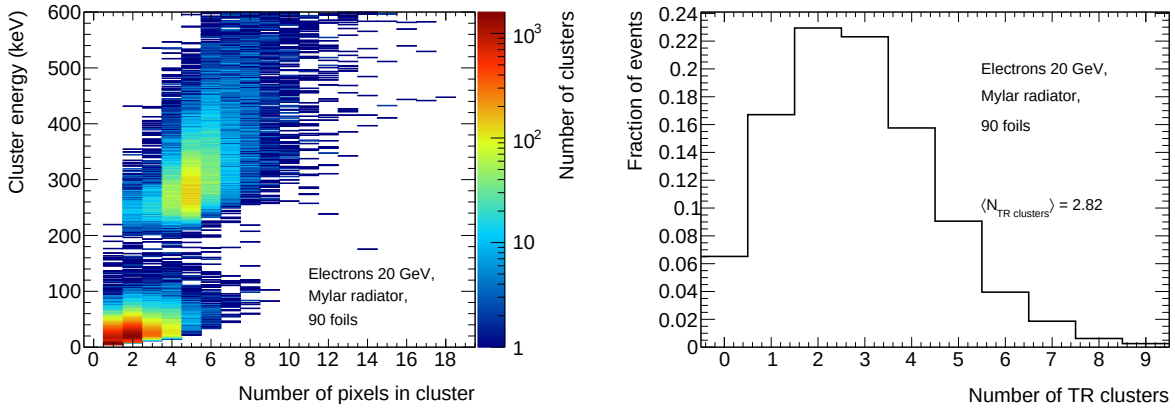

(a) (b)

Figure 2. Distribution of cluster energy against cluster size (a) and distribution of the number of TR clusters per charged particle (b). Experimental conditions: 20 GeV/c electrons, 90-foil Mylar radiator.

4. Detector simulation model

The MC model used in this work is similar to that described in our earlier work for a Si sensor [7]. It includes a simulation of the physics processes and the detector response. The simulation of the transition radiation and the multiple scattering of particles traversing the radiator is done in the same way as for the Si detector. However, there are a few essential differences in the simulation of the GaAs sensor with respect to that of the Si one. First of all, both GaAs sensor materials have about 50% yield of fluorescent photons with energies of 9.2 keV (Ga) and 10.5 keV (As). These photons have 40.6 μm and 16.6 μm absorption lengths, respectively, and may escape from the main cluster area producing separate clusters. Ionization electrons produced in the detector drift towards the anode, while holes, contrary to what happens in Si detectors, are quickly trapped and do not participate in the signal formation. There is also a rather high probability for electrons to be trapped during the drift. This effect is strong for low bias voltages. However, for the bias voltage of −450 V used in the tests, more than 90 % of charge is collected. Effects of charge collection efficiency are taken into account by energy calibration. Finally, the diffusion of a drifting charge is higher in GaAs detectors than in Si ones (the sigma of the charge distribution is 9 μm versus 3 μm [7] for 500 μm drift length), and therefore the charge sharing effect is significantly larger. After the charge is collected by each pixel, the electronics noise is added by smearing the energy associated to each pixel using a Gaussian distribution with a σ of 426 eV (100 primary electrons). The latter value is considered as the noise level of each pixel expressed in energy units. This value is slightly larger than the noise of the electronics because it includes a spread of pixel thresholds. The average electronics threshold used in the test-beam studies was equivalent to 4.2 keV. The fraction of charge collected by a pixel will be lost if it is below this threshold. Because of a relatively large leakage current in GaAs detectors, a decay time of the signal from a pre-amplifier is significantly shorter than that in Si sensors. This leads to an increase of the effect of the ToT measurement binning. In order to take this effect into account, signals which passed the threshold criteria were smeared further with the Gaussian distribution with a σ of 1.2 keV. Finally, a calibration procedure similar to that described above for data was carried out.

In order to take into account secondary processes leading to production of photons and delta electrons along the beam line, special runs with a "dummy" radiator (3 mm thick polyethylene slab) were taken. Clusters obtained in these runs were added to those obtained in the simulations,

with a proper scaling factor to account for the different number of events. This procedure also allows to take into account clusters from fluorescent photons produced by the particle in ionization processes.

The surface of the GaAs sensors is covered by 1 μm Ni [10] which absorbs a fraction of soft TR photons. During sensor production the treatment of the GaAs crystal may deteriorate surface properties and lead to a formation of a thin dead layer. Ionization produced in these layers will be lost, but fluorescent photons may escape from this layer and can be detected as separate photon clusters. Thin absorption layers mostly affect the soft part of the spectrum (below 15 keV). It was found that in order to reach a good agreement with data, a 3 μm GaAs dead layer should be introduced. The results of the simulation are compared with the data using 20 GeV/c electron runs with the 30 and 90 foils Mylar radiator, whose parameters are measured with high accuracy, and which exhibits negligible fluctuations in the thicknesses of the foils and the air gaps.

5. Simulation and data comparison

The TR photon cluster reconstruction efficiencies as a function of the distance from the beam particle cluster for Data and MC are shown in figure 3 (a). These efficiencies are calculated as the fraction of events for which a pixel at a given distance from the beam particle cluster position belongs to a TR photon cluster. At a distance equivalent to 3 times the pixel pitch, the efficiency of TR cluster reconstruction is about 80%. Above this distance more than 95% efficiency is reached and the beam particle cluster and the TR photon cluster will always be separated. The distance of 3 pixels corresponds to 165 μm, and makes it possible to detect TR photons at angles down to 0.75 mrad if the TR photon emission occurs 2 m before the detector. Figure 3 (b) shows the measured energy distribution of TR clusters compared with the MC predictions for the 30 foils Mylar radiator. The figure also shows the MC predictions obtained without including the background contribution measured in the runs with the "dummy" radiator.

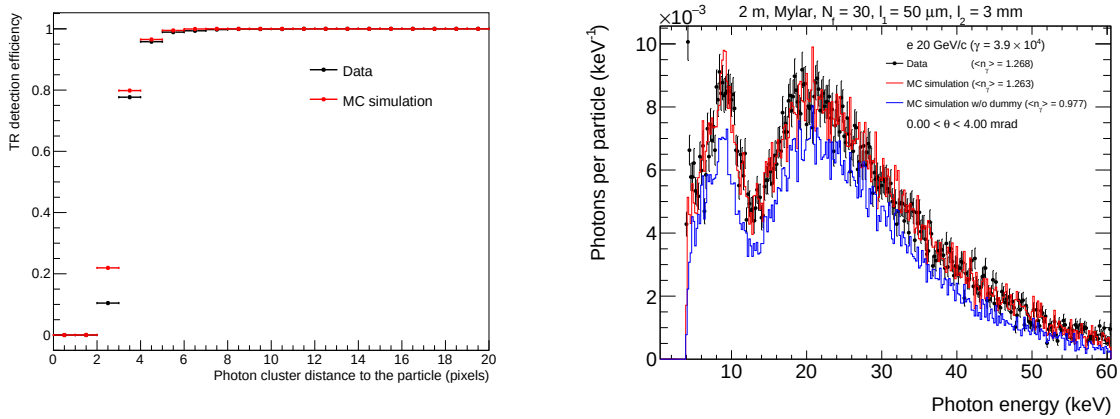

(a) (b)

Figure 3. Reconstruction efficiencies of TR clusters for Data and MC as a function of the distance from the particle cluster (a) and Data/MC comparison of cluster energy spectra with and without "dummy" radiator (b). Experimental conditions: 20 GeV/c electrons, 30-foil Mylar radiator. Symbol $\langle n_\gamma \rangle$ denotes mean number of TR photons per particle.

The measured double-differential TR photon spectrum for the 30 foil Mylar radiator as a function of emission angle and photon energy is compared with the one obtained from the MC simulation in figure 4. Figure 4 (a) refers to experimental data, while figure 4 (b) refers to the MC simulation.

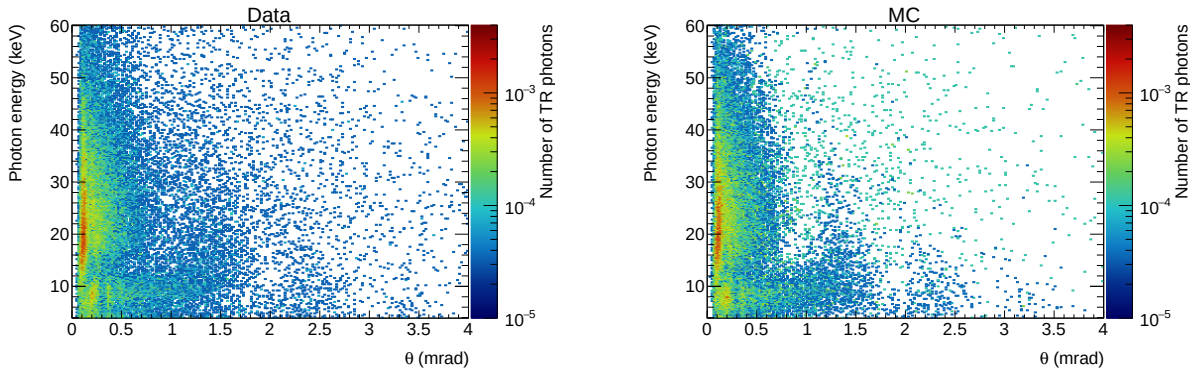

(a) (b)

Figure 4. Two dimensional distributions of photon energy versus reconstructed production angle obtained with the 30 foil Mylar radiator for 20 GeV/c electrons for Data (a) and MC simulations (b). Z-axis is a number of photons per particle.

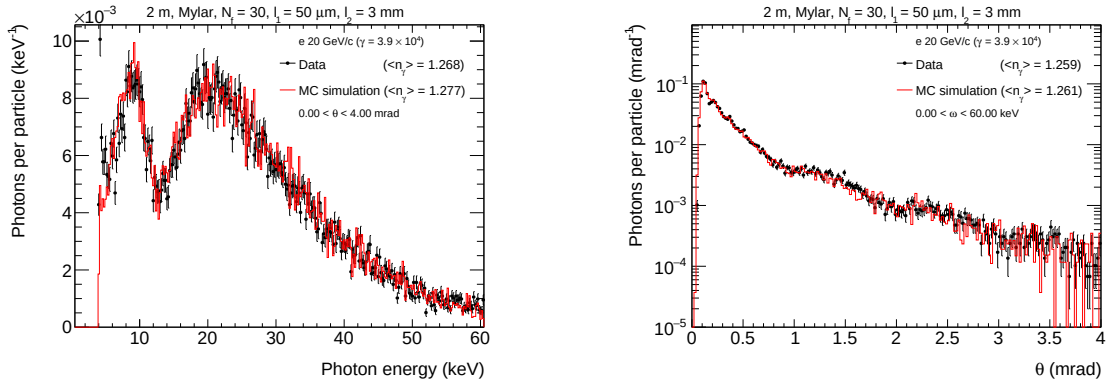

(a) (b)

Figure 5. Comparison between the measured and simulated TR differential energy (a) and angular (b) spectra obtained with the 30 foils Mylar radiators. Electron beam energy 20 GeV/c.

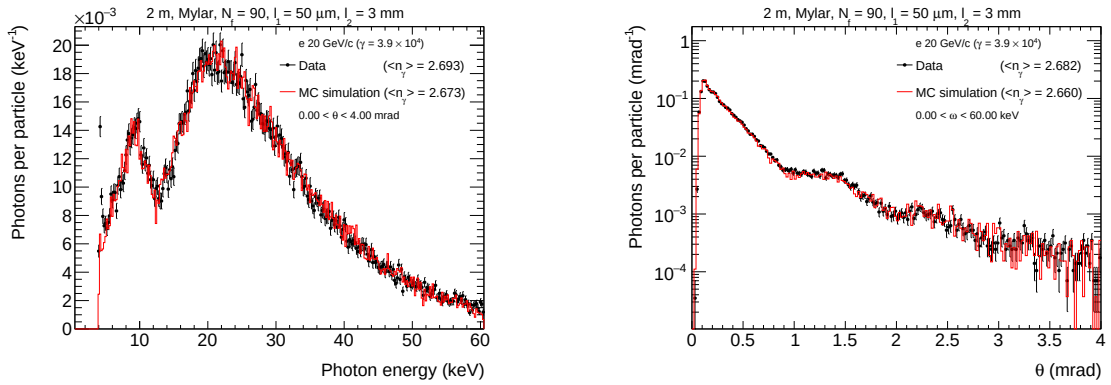

(a) (b)

Figure 6. Comparison between the measured and simulated TR differential energy (a) and angular (b) spectra obtained with the 90 foils Mylar radiators. Electron beam energy 20 GeV/c.

From the plots above, one concludes that for the Mylar radiator made of 50 μm foils there are two main families of TR photons. The first one corresponds to photons with energies $E_\gamma > 13\,\text{keV}$ emitted at angles $\theta < 0.5\,\text{mrad}$, while the second one corresponds to photons in the remaining region of the (θ, E_γ) plane. It is important to note that these two families have different gamma factor dependencies (see [7]).

Details of the energy and the angular distributions of the TR photons for Mylar radiators with 30 and 90 foils and a comparison with the MC simulations are presented in figures 5 and 6, respectively. Figures 5 (a) and 6 (a) show the energy distributions, while figures 5 (b) and 6 (b) show the angular distributions. These results are obtained with $20\,\text{GeV/c}$ electrons. These figures show that simulations reproduce the experimental data correctly, even in details. No special parameter tuning, except what was described in the sections above, was done. For the 90 foils radiator one sees that the multiple scattering significantly smears the interference peaks.

6. Conclusions

The Timepix3 pixel front-end chips attached to a high quality GaAs sensors allow to build efficient X-ray detectors with high spatial resolution and good energy resolution. This offers the possibility to detect X-ray transition radiation photons and separate them from the particle ionization clusters. A MC simulation model of the detector response was developed and shows good agreement with the data. This model provides reliable simulation of the TRD configurations for different applications.

Acknowledgments

We gratefully acknowledge the financial support from Russian Science Foundation grant (project No. 16-12-10277).

References

[1] Zyla P *et al.* (Particle Data Group) 2020 *PTEP* **2020** 083C01
[2] Dolgoshein B 1993 *Nucl. Instrum. Methods Phys. Res.* A **326** 434–69
[3] Andronic A and Wessels J 2012 *Nucl. Instrum. Methods Phys. Res.* A **666** 130–47 (*Preprint* 1111.4188)
[4] Albrow M 2018 *PoS* **EDSU2018** 048
[5] Belyaev N *et al.* 2017 *J. Phys. Conf. Ser.* **934** 012053
[6] Belyaev N *et al.* 2019 *J. Phys. Conf. Ser.* **1390** 012126
[7] Alozy J *et al.* 2020 *Nucl. Instrum. Methods Phys. Res.* A **961** 163681
[8] Ballabriga R, Campbell M and Llopart X 2018 *Nucl. Instrum. Methods Phys. Res.* A **878** 10–23
[9] Dachs F *et al.* 2020 *Nucl. Instrum. Methods Phys. Res.* A **958** 162037
[10] Smolyanskiy P *et al.* 2018 *J. Instrum.* **13** T02005 (*Preprint* 1712.03369)
[11] Poikela T *et al.* 2014 *J. Instrum.* **9** C05013
[12] Burian P *et al.* 2017 *J. Instrum.* **12** C11001
[13] Jakubek J 2011 *Nucl. Instrum. Methods Phys. Res.* A **633** S262 – 6
[14] Kiehn M *et al.* 2019 Proteus beam telescope reconstruction URL https://doi.org/10.5281/zenodo.2586736